Exploring experimental and computational markers of cyclic peptides: Charting islands of permeability

ARTICLE *in* EUROPEAN JOURNAL OF MEDICINAL CHEMISTRY · JUNE 2015

Impact Factor: 3.45 · DOI: 10.1016/j.ejmech.2015.04.049

8 AUTHORS, INCLUDING:

Joakim Swedberg
University of Queensland
35 PUBLICATIONS **269** CITATIONS
SEE PROFILE

Stephanie Chaousis
Griffith University
8 PUBLICATIONS **30** CITATIONS
SEE PROFILE

David Price
Pfizer Inc.
53 PUBLICATIONS **2,219** CITATIONS
SEE PROFILE

Spiros Liras
Pfizer Inc.
74 PUBLICATIONS **1,632** CITATIONS
SEE PROFILE

European Journal of Medicinal Chemistry 97 (2015) 202–213

Contents lists available at ScienceDirect

European Journal of Medicinal Chemistry

journal homepage: http://www.elsevier.com/locate/ejmech

Exploring experimental and computational markers of cyclic peptides: Charting islands of permeability

Conan K. Wang [a, 1], Susan E. Northfield [a, 1], Joakim E. Swedberg [a], Barbara Colless [a], Stephanie Chaousis [a], David A. Price [b], Spiros Liras [b], David J. Craik [a, *]

[a] Institute for Molecular Bioscience, The University of Queensland, Brisbane, Queensland 4072, Australia
[b] Worldwide Medicinal Chemistry, CVMED, Pfizer, 610 Main Street, Cambridge, MA 02139, USA

ARTICLE INFO

Article history:
Received 8 April 2015
Received in revised form
23 April 2015
Accepted 24 April 2015
Available online 25 April 2015

Keywords:
Peptide
Cyclic peptide
Drug design
NMR
Amide temperature coefficients

ABSTRACT

An increasing number of macrocyclic peptides that cross biological membranes are being reported, suggesting that it might be possible to develop peptides into orally bioavailable therapeutics; however, current understanding of what makes macrocyclic peptides cell permeable is still limited. Here, we synthesized 62 cyclic hexapeptides and characterized their permeability using *in vitro* assays commonly used to predict *in vivo* absorption rates, i.e. the Caco-2 and PAMPA assays. We correlated permeability with experimentally measured parameters of peptide conformation obtained using rapid methods based on chromatography and nuclear magnetic resonance spectroscopy. Based on these correlations, we propose a model describing the interplay between peptide permeability, lipophilicity and hydrogen bonding potential. Specifically, peptides with very high permeability have high lipophilicity and few solvent hydrogen bond interactions, whereas peptides with very low permeability have low lipophilicity or many solvent interactions. Our model is supported by molecular dynamics simulations of the cyclic peptides calculated in explicit solvent, providing a structural basis for the observed correlations. This prospective exploration into biomarkers of peptide permeability has the potential to unlock wider opportunities for development of peptides into drugs.

1. Introduction

Peptides are promising drug leads because of their potential to simultaneously offer the advantages of small molecule therapeutics and large protein biologics [1]. Peptides can bind with exquisite specificity to their *in vivo* targets, resulting in exceptionally high potencies and relatively few off-target side-effects. Additionally, their small size compared to proteins suggests that they might adopt the favorable pharmacological properties that are commonly associated with small molecule therapeutics, such as oral bioavailability.

Achieving high oral bioavailability for peptide drugs is still perceived to be a challenging task and is a key design objective in the pharmaceutical industry, especially for chronic treatments. This challenge has translated to wide interest in drug design guidelines to help alleviate the often huge effort required to develop a successful oral therapy. Principles for designing orally bioavailable small molecule therapeutics have been described in the widely referenced 'Lipinski Rule of Five' [2]. Other guidelines to assess 'drug-likeness' or 'lead-likeness' have subsequently been established [3], which note the importance of polar surface area, among other criteria [4]. These guidelines have been most useful in understanding the properties of small molecule compounds that are associated with oral bioavailability but have led to the perception that peptides make poor drugs because they occupy an unconventional physico-chemical space.

We envisage that peptide and peptidomimetic macrocycles have the potential to fill a gap in the chemical space between small molecules and protein therapeutics and thus emerge as a modality for difficult targets. This view is supported by a growing number of peptides that appear to be well absorbed within the gastrointestinal tract [5] and examples where cyclic peptides have shown orally-delivered bioactivity in animal models of disease, including inflammatory pain [6] and neuropathic pain [7]. Interestingly, a common structural feature of these reported peptides is a

* Corresponding author. Institute for Molecular Bioscience, The University of Queensland, Brisbane, Queensland, 4072, Australia.
E-mail address: d.craik@imb.uq.edu.au (D.J. Craik).
[1] These authors contributed equally.

http://dx.doi.org/10.1016/j.ejmech.2015.04.049
0223-5234/

macrocyclic backbone, which is consistent with a study showing that cyclic peptides have improved membrane permeability over their linear counterparts [8]. Cyclization is important for oral bioavailability presumably because it improves stability against proteolytic degradation and also directs the peptide into specific conformations that might be favorable for membrane permeability [8–10]. Arguably the most famous example of a cyclic peptide with reasonable oral bioavailability yet poor drug-likeness is cyclosporin A (CSA), which was originally discovered from a soil fungus and is now widely used as the immunosuppressant cyclosporine [11].

Backbone N-methylation is another structural feature, aside from cyclization, that seems to be correlated with improved membrane permeability [12]. Indeed, N-methylation of a cyclic peptide agonist of somatostatin improved its oral bioavailability without significantly modifying its biological activity and selectivity [13]. In some cases, N-methylation does not increase membrane permeability and arbitrarily increasing the number of N-methyl modifications is not reflected by the sought-after increase in permeability [14]. Recently, strategic incorporation of N-methyl groups using either an on-resin chemical approach [15] or a structure-informed approach has led to the development of cyclic peptides with small molecule-like oral bioavailability [16]. In the structure-informed approach, amide temperature coefficients measured by NMR were used to identify appropriate amides to modify. Both of these approaches recognize the intricate relationship between N-methylation and the role of unmodified amides in the formation of intra-molecular and solvent hydrogen bonds. The importance of hydrogen bonding potential of cyclic peptides is supported by a recent study [17], where the relative rates of diffusion of 11 closely-related cyclic hexapeptides across an artificial membrane were found to correlate with *in silico* estimates of the solvation free energies associated with their predicted aqueous and membrane-associated conformations.

A key objective of this study was to define the properties that influence permeability of cyclic peptides. Here we correlate the *in vitro* permeability of peptides with their physico-chemical properties (Fig. 1). We synthesized and purified a library of 62 hexapeptides with varying sequence composition and N-methylation content. We focused on convenient and rapid experimental techniques to characterize the lipophilicity (e.g. analytical chromatography) and hydrogen bonding potential (e.g. NMR amide temperature coefficients) of the peptides. Although amide temperature coefficient experiments have been used previously to provide Supplementary information in structural studies of proteins, their potential as experimental markers of peptide permeability has not been studied. Based on these measurements, we developed a model describing the interplay between peptide lipophilicity and hydrogen bonding potential that can be assessed by experimental means. Our model is supported by molecular dynamics simulations of the peptides in explicit solvent, relating our experimentally-derived observations to predicted structures.

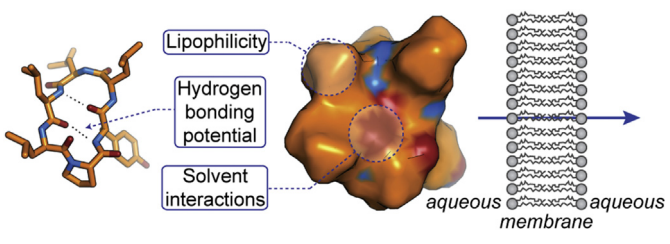

Fig. 1. Markers of peptide permeability across a membrane. Using computational and experimental tools, we examined various physico-chemical properties of peptides, e.g. their lipophilicity and hydrogen bonding potential, and correlated these properties to membrane permeability. A stick and surface representation of the predicted structure of a cyclic hexapeptide studied in this work is shown; carbon atoms are colored orange, oxygen atoms are shown in red, and nitrogen atoms are colored blue. (For interpretation of the references to color in this figure legend, the reader is referred to the web version of this article.)

2. Experimental section

2.1. General

Fmoc-protected amino acids, resins and coupling agents were purchased from ChemImpex International. All other reagents were purchased from Auspep, Merck and Sigma, and used without further purification.

2.2. Peptide synthesis

Linear peptides were synthesized on 2-chlorotrityl chloride (2CTC)resin. Couplings were performed using 4 equiv. Fmoc-protected amino acid, 3 equiv. HATU (*O*-(7-azabenzotriazol-1-y1)-*N,N,N′,N′*-tetramethyluroniumhexafluorophosphate) or HCTU (*O*-(1*H*-6-chlorobenzotriazol-1-y1)-*N,N,N′,N′*-tetramethyluro-nium hexafluorophosphate) and 6 equiv. N,N-diisopropylethylamine (DIPEA) in dimethylformamide (DMF) for 0.5–2 h. Fmoc deprotection was carried out with 30% (v/v) piperidine in DMF. After each coupling and deprotection step, the resin was washed with DMF (3×), dichloromethane (DCM) (3×) and DMF (3×). Peptides were cleaved from the resin using 1% (v/v) TFA (trifluoroacetic acid) in DCM (dichloromethane). Head-to-tail cyclization was performed in DMF with 3 equiv. HATU and 6 equiv. DIPEA. Following removal of the solvent, side-chain protecting groups were removed in 94:3:3 TFA/TIPS (triisopropylsilane)/water. After cyclization, the peptides were purified by reverse-phase preparative HPLC. Purity of fractions was assessed using ESI-MS and analytical HPLC.

2.3. PAMPA for determining passive cell permeability

A 96-well donor and accepter plate system pre-loaded with artificial lipid membrane (BD Gentest™ Pre-coated PAMPA Plate) was used. In these plates, each well consists of a polyvinylidene fluoride (PVDF) filter coated with a lipid/oil/lipid trilayer, where the lipid layer is composed of 1,2-dioleoyl-*sn*-glycero-3-phosphocholine and the oil layer is composed of hexadecane [18].

300 μL of 50 μM peptide (5% (v/v) DMSO in Hank's Balanced Salt Solution [HBSS])was added to the donor wells and 200 μL of buffer (5% (v/v) DMSO in HBSS) was added in the acceptor wells. The acceptor plate was lowered onto the donor plate so that the artificial membrane was in contact with the peptide solution below. A cover plate was placed on the acceptor plate and the assay plate covered with foil. Incubation of peptides was carried out at room temperature for 5 h.

Acceptor and donor well concentrations were measured using an UHPLC/MS system equipped with a C18 Kinetex (2.10 × 50 mm, 7 μm). The eluant was acetonitrile/water 10/90 with 0.045% v/v formic acid and was pumped through the column at 0.4 mL min^{-1}. The visible spectra were recorded at 214 and 280 nm. Mass spectrometer parameters were set as follows for positive ion mode: gas temperature 250 °C; drying gas (N_2), 15 L min^{-1}; capillary voltage 4.5 kV. The mass range used for selective ion monitoring was changed depending on the peptide.

As the concentration differences between acceptor and donor wells are significant, they were analyzed separately. Dilution series of each peptide sample were prepared and injected into the LC-MS to generate a standard curve for quantification. Five μL from donor or 40 μL from acceptor wells were injected into the LC-MS and the analyte peak areas were recorded. The limit of detection of the peptides varies; however, most gave a value of ~0.05 μM.

Percentage permeability was calculated relative to the equilibrium concentration.

The permeability coefficient ($P_{app\text{-}pampa}$) values were calculated according to the equation:

$$P_{app-pampa} = \frac{-\ln\left[1 - C_A \big/ C_{equilibrium}\right]}{A \times (1/V_D + 1/V_A) \times t}$$

Where C_A is the sampled concentration in the acceptor compartment, V_A is the volume in the acceptor compartment, V_D is the volume of the donor compartment, t is the incubation time, A is the area of the filter and:

$$C_{equilibrium} = [C_D \times V_D + C_A \times V_A]/(V_D + V_A)$$

Each PAMPA measurement was typically an average of triplicates and repeated to n = 3. For some peptides with low permeability (e.g. $P_{app\text{-}pampa} < 0.1 \times 10^{-6}$ cm/s), measurements were not repeated more than n = 2. Permeability values could not be determined for peptides **29**, **30**, **31**, and **46** due to poor sample solubility.

2.4. Caco-2 permeability studies

Caco-2 cells were cultured in an atmosphere of 5% CO_2 and 90% relative humidity in T75 flasks (Nunc) with 10 mL of media (10% fetal bovine serum (FBS), 1% non-essential amino acids (NEAA), 1% penicillin/streptomyocin). Cells were passaged 1:10 every five days, or when 80–90% confluent, using 0.25% trypsin-EDTA (Invitrogen, Gibco Laboratories). Caco-2 cells were seeded onto each membrane of the transwell permeable support 12-well plate insert to give 50,000 cells/well. The individual feeding tray wells received 1.5 mL of cell culture medium. The cell culture medium was changed every second day. Caco-2 cell monolayers were used for experimentation 21 days post-seeding. To prepare the cells for transport studies (apical to basolateral, A to B) cell culture media was removed from both compartments and the cells were washed once with HBSS in both the A and B compartments. The washing buffer was removed and 0.75 mL of fresh HBSS placed in compartment A and 1.5 mL of HBSS in compartment B for pre-incubation, carried out at 37 °C for 30 min under agitation. Transepithelial electrical resistance (TEER) was measured across the cell membranes at the beginning of the experiment. HBSS was subsequently removed from compartment A, replaced with 0.75 mL of the peptide solution prepared in HBSS. Monolayers were incubated and continuously shaken. 100 μL samples were taken from the A and B compartments at 45 min and 90 min intervals, and the buffer volume replenished. After 90 min, 200 μL of compartment A and B was also collected for Lucifer Yellow (LY) measurements. Amount of LY permeated was measure on a Tecan plate reader (excitation 485 nm, emission 530 nm). At the conclusion of the experiment TEER was measured again to confirm the integrity of the Caco-2 monolayers (TEER >300 Ω cm^2). Acceptor and donor well concentrations were measured by LC-MS as per the PAMPA Assay.

The permeability coefficient ($P_{app\text{-}caco}$) values were calculated according to the equation:

$$P_{app-caco} = \frac{V_A}{t} \times \frac{C_A}{C_0} \times \frac{1}{A}$$

Where C_A is the sampled concentration in the acceptor compartment, V_A is the volume in the acceptor compartment, t is the incubation time, C_0 is the initial concentration in the donor compartment, and A is the area of the filter of the transwell plate. Each Caco-2 measurement was typically an average of triplicates and repeated to n = 3. For permeability values less than 1×10^{-6} cm/s, some samples were not repeated more than n = 2. Permeability values could not be determined for peptides **29**, **30** and **31** due to poor sample solubility.

2.5. Retention time measurements

Samples were analyzed using RP-HPLC. A Phenomenex Jupiter 5 μm C18 300 Å 150 × 2 mm column was employed, with a flow rate of 0.3 mL/min at 25 °C. A solvent gradient was employed as follows: 5% B over 5 min, 5–100% B over 47.5 min (Solvent B was composed of 90% v/v acetonitrile, 9.95% v/v water, 0.05% TFA). An early-eluting peptide (Ac-Pro-Glu-Glu-Leu-Gly-Leu-Asp-Gly-Lys-OH) and a late-eluting peptide (peptide **12**) were added to each sample prior to injection. Peptide samples were dissolved in DMSO to a final concentration of ~0.1 mM.

2.6. Amide temperature coefficient studies

The temperature dependence of amide proton chemical shifts was derived from 1D and TOCSY spectra recorded on a Bruker Avance 500 MHz spectrometer. Spectra were measured between 288 K and 308 K, in 5 K increments, and referenced to DSS at 0 ppm. Assignment of the spectra was performed using the program rNMR [19] and/or CCPNMR [20].

2.7. Translational diffusion coefficient studies

Translational diffusion coefficients were measured as described previously [21]. Briefly, PFG-NMR spectra were acquired at 25 °C on a Bruker Avance 500 MHz spectrometer. Diffusion coefficients were measured by incrementing either the duration of the field gradient pulses or the amplitude while the separations of the field gradients and the total echo time remained constant.

2.8. Quantitative Structure Activity Relationship (QSAR) studies

QSAR analyses were performed using an in-house spreadsheet embedded with QSAR routines. Prior to fitting, the descriptor values were auto-scaled by subtracting the mean and dividing the resultant values by the standard deviation.

2.9. Molecular dynamics analysis

Cyclic hexapeptides were generated using CYANA [22] using only *cis*/*trans* peptide bond constraints (identified from the NMR spectra) producing 20 low energy conformers/peptide. Structures with near identical conformations were removed from the pools, resulting in 4–10 unique conformations per peptide. The peptides were solvated in 30% acetonitrile using YASARA v.13.9.8 [23] and produced systems of 600–700 TIP3 water and 100–150 acetonitrile molecules. Simulation topology files were prepared using VMD 1.9.1 [24] and the CHARMM27 topologies. For acetonitrile the CGenFF 2b8 topology [25] was used, whereas custom topologies for N-methylated amino acids were constructed using SwissParam [26].

Each solvated peptide was equilibrated using a stepwise relaxation procedure. In the first stage, all heavy-atoms were harmonically restrained with a force constant of 2 kcal/(mol $Å^2$) before a conjugate gradient minimization of 500 steps was applied using NAMD 2.9 CUDA [27] and CHARMM27 force field parameters. N-methyl parameters were constructed as described for topologies above. This was followed by heating to 298 K before simulating 500 ps under NPT conditions with periodic boundary conditions. A Langevin thermostat with a damping coefficient of 0.5 ps^{-1} was

used to maintain the system temperature. The system pressure was maintained at 1 atm using a Langevin piston barostat. The particle mesh Ewald algorithm was used to compute long-range electrostatic interactions at every time step and non-bonded interactions were truncated smoothly between 10 Å and 12 Å. All covalent hydrogen bonds were constrained by the SHAKE algorithm (or the SETTLE algorithm for water), permitting an integration time step of 2 fs. For the second stage of 1 ns, the restraints were retained on α-carbons (Cα) only, whereas all constraints were released in the third stage of 1 ns. Production runs were simulated for 10 ns while saving 10,000 evenly spaced frames for each simulation.

The hydrogen bond patterns during the last equilibration trajectory step determined using the HBonds Plugin v. 1.2 in VMD (bond lengths and angles set to 3.3 Å and 40°, respectively). The bond angle was chosen based on a study of over 4500 protein crystal structures which found that over 80% of protein backbone *NH–O* hydrogen bonds fall within a <40° cut-off [28]. The conformation variant of each peptide that most closely aligned with temperature coefficients determined by NMR was selected for production runs. As the starting structures of the peptides were based on experimentally-derived data, we did not expect substantial conformational changes to occur and chose to conduct production runs of 10 ns. Subsequent hydrogen bond analysis were performed for all saved frames and peptides as described above. The biophysical properties and Cα RMSD variations of peptides were determined using VEGA ZZ v. 3.0.2.48 [29] (Probe radius 1.4 Å; resolution 10; 10,000 frames per peptide) and MUSTANG [30] in YASARA respectively. The average peptide simulation structures from the production trajectories in 30% acetonitrile were solvated in chloroform, parameterized, equilibrated, simulated and analyzed as described above.

3. Results

3.1. Design and synthesis of cyclic hexapeptides

The sequences of the cyclic peptides synthesized for this study are detailed in Fig. 2, and are divided into three groups. Group 1 contains cyclic hexapeptides with the general sequence, cyclo(Leu-Leu-Leu-Leu-Pro-Tyr) [10], but have varied chirality and N-methylation configurations, and therefore are expected to have varied conformations. Some of these peptides have been reported to have high *in vitro* and *in vivo* permeability; peptides **12** (referred to as **3** in Ref. [15]) and **13** (referred to as **15** in Ref. [16]), for example, both displayed oral bioavailability greater than 20%, which is unusually high for peptides. Group 2 comprises peptides with a similar range of chirality and N-methylation configurations as those in Group 1, but was designed to explore the effect of sequence variation on peptide permeability. Group 3 contains cyclic hexapeptides with a greater range of sequence variation compared to Group 2, and are mainly derived from the orbitides – a family of naturally-occurring cyclic peptides from plants [31]. These peptides were included in this study to examine the potential permeability of naturally-occurring cyclic peptides. In total, we examined 62 different cyclic hexapeptides to begin exploring experimental and computational markers of peptide permeability.

3.2. In vitro permeability studies

We analyzed the membrane permeability of our suite of cyclic peptides across a Caco-2 cell monolayer (Supplementary Table 1), a cell-based system that incorporates both active and passive transport mechanisms. Similarly, we assessed the permeability of our peptides using PAMPA (Supplementary Table 1), which is used to determine the passive membrane permeability of analytes through an artificial phospholipid membrane and correlates well to *in vivo* absorption rates [32]. We observed a positive correlation between Caco-2 and PAMPA permeability ($r^2 = 0.72$), as shown in Fig. 3, suggesting that the cyclic peptides in this study mostly engage in passive transport pathways.

3.3. HPLC capacity factor as a predictor of permeability

Measurement of retention times is a rapid and convenient way to probe the surface properties of an analyte, and has recently been used to study the surface hydrophobicity of cyclic alanine-rich peptides [9]. In fact, retention time measurements converted to their respective capacity factors (and more specifically the logarithm of the capacity factors, log k′) have been widely used as a method for estimating lipophilicity [33]. To begin exploring experimental markers, we first correlated the retention times of the peptides on reversed-phase high performance liquid chromatography (RP-HPLC) to their observed Caco-2 and PAMPA permeability, as shown in Fig. 4A and B, respectively, as well as to their recovery from the permeability assays, as shown in Supplementary Fig. 1. Fig. 4C shows a typical RP-HPLC chromatogram acquired using acetonitrile as the organic component of the mobile phase; for each sample, we added an early-eluting and a late-eluting peptide to calibrate measurements between samples. We then calculated the capacity factors (as log k′; Supplementary Table 2) and correlated them to their Caco-2 and PAMPA permeability, as shown in Fig. 4D and E, respectively. Noticeably, there is a positive correlation between log k′ and the logarithm of the apparent permeability value measured using the Caco-2 assay ($r^2 = 0.75$; Fig. 4D). For the PAMPA result shown in Fig. 4E, permeability of the cyclic peptides also increases with increasing log k′ ($r^2 = 0.77$ for log k′ ≤ 1.3). In contrast, the correlation appears to invert for log k′ > 1.3; although the correlation is weak (i.e. $r^2 = 0.32$), this behavior would be consistent with that reported for hydrophobic compounds that passively diffuse across a artificial membranes [34,35]. Nevertheless, the apparent dependence of cyclic peptide permeability on log k′ suggests that the capacity factor (or, in principle, retention time) can be used as a 'filter' to guide the design of membrane-permeable peptides. More specifically, peptides that eluted before 30 min (or had a log k′ less than approximately 1.23) showed very low permeability (Fig. 4A and B–E). Interestingly though, not all peptides that eluted after 30 min displayed high permeability in both Caco-2 (Fig. 4A) and PAMPA (Fig. 4B) assays, inspiring us to search for other experimental markers that might explain the differences in the observed rates of peptide diffusion across membranes.

3.4. Amide temperature coefficients and hydrogen bonding potential as predictors of permeability

To clarify whether the hydrogen bonding potential of peptides affects their *in vitro* permeability, we examined basic properties of the peptides that could be easily ascertained from their representative chemical structures, such as the number of hydrogen bond donors, hydrogen bond acceptors and N-methylated amides. Although some of these properties have been used to guide the design of small-molecule therapeutics, we found no clear correlation between any of these properties and the permeability of the peptides (Supplementary Fig. 2). We reasoned that since the solution conformation will have a different number of 'available' hydrogen bond donors and acceptors to that predicted based on their two-dimensional chemical representation, experimental measurement of the hydrogen bonding potential of the peptides would be a more useful and meaningful biomarker of peptide permeability.

To do this, we investigated the utility of NMR chemical shift

Group 1 (Leu-rich)

cyclic peptide	residue position 1	2	3	4	5	6
1	Leu	D-Leu	D-Leu	D-Leu	Pro	Tyr
2	Leu	Leu	D-Leu	D-Pro	Pro	Tyr
3	D-Leu	D-Leu	D-Leu	Leu	Pro	Tyr
4	D-Leu	D-Leu	Leu	D-Leu	Pro	Tyr
5	Leu	D-Leu	Leu	Leu	D-Pro	Tyr
6	Leu	D-Leu	Leu	Leu	D-Pro	Tyr
7	Leu	D-Leu	Leu	Leu	D-Pro	Tyr
8	Leu	D-Leu	Leu	Leu	D-Pro	Tyr
9	Leu	D-Leu	Leu	Leu	D-Pro	Tyr
10	Leu	D-Leu	Leu	Leu	D-Pro	Tyr
11	Leu	D-Leu	Leu	Leu	D-Pro	Tyr
12	Leu	D-Leu	Leu	Leu	D-Pro	Tyr
13	Leu	D-Leu	D-Leu	D-Leu	Pro	Tyr
14	Leu	Leu	D-Leu	D-Pro	Pro	Tyr
15	D-Leu	D-Leu	D-Leu	Leu	Pro	Tyr
16	D-Leu	D-Leu	Leu	D-Leu	Pro	Tyr
17	Leu	D-Leu	Leu	Leu	D-Pro	Tyr
18	Leu	Leu	D-Leu	D-Pro	Pro	Tyr
19	D-Leu	D-Leu	Leu	D-Leu	Pro	Tyr
20	D-Leu	Leu	Leu	Leu	Pro	Tyr
21	D-Leu	Leu	Leu	Leu	Pro	Tyr
22	Leu	D-Leu	Leu	D-Leu	D-Pro	Tyr
23	Leu	D-Leu	D-Leu	D-Leu	Pro	Trp
24	Leu	Leu	D-Leu	D-Pro	Pro	Trp
25	D-Leu	D-Leu	D-Leu	Leu	Pro	Trp
26	D-Leu	D-Leu	Leu	D-Leu	Pro	Trp
27	Leu	D-Leu	Leu	Leu	D-Pro	Trp
28	Ile	D-Leu	Ile	Ile	D-Pro	Trp

Group 2 (Sequence variants)

cyclic peptide	residue position 1	2	3	4	5	6
29	Phe	D-Phe	Phe	Phe	D-Pro	Trp
30	Leu	D-Leu	Trp	Leu	D-Pro	Trp
31	Leu	Leu	Trp	Trp	D-Pro	Trp
32	D-Trp	Lys	Thr	Phe	Pro	Phe
33	D-Trp	D-Lys	Thr	D-Phe	Pro	Phe
34	Ala	Gly	Phe	Leu	D-Pro	Tyr
35	D-Ala	Gly	Phe	D-Leu	Pro	Tyr
36	D-Ala	Gly	Phe	D-Leu	Leu	Tyr
37	Ala	Gly	D-Phe	D-Leu	Pro	Tyr
38	D-Ala	Gly	D-Phe	Leu	Pro	Tyr
39	D-Ala	Gly	Phe	Leu	Pro	Tyr
40	Ala	Gly	Phe	Leu	D-Pro	Tyr
41	Ala	Gly	Phe	Leu	D-Pro	Tyr
42	D-Ala	Gly	Phe	D-Leu	Pro	Tyr
43	D-Ala	Gly	Phe	D-Leu	Leu	Tyr
44	Ala	Gly	D-Phe	D-Leu	Pro	Tyr
45	D-Ala	Gly	D-Phe	Leu	Pro	Tyr
46	D-Ala	Gly	Phe	Leu	Pro	Tyr
47	Leu	Gly	Phe	Leu	Pro	Tyr
48	Leu	D-Leu	Phe	Leu	Pro	Tyr
49	Arg	D-Arg	Arg	Lys	D-Pro	Trp
50	D-Ala	Ala	Ala	Ala	Ala	Ala

Group 3 (Orbitide-like)

cyclic peptide	residue position 1	2	3	4	5	6
51	Pro	Phe	Phe	Trp	Val	Leu
52	Pro	Phe	Tyr	Pro	Gly	Leu
53	Pro	Gly	Leu	Val	Ile	Tyr
54	Gly	Thr	Phe	Leu	Tyr	Val
55	Gly	Val	Gly	Phe	Tyr	Ile
56	Gly	Thr	Phe	Leu	Tyr	Ala
57	Ala	Tyr	Asn	Phe	Gly	Leu
58	Gly	Thr	Phe	Leu	Tyr	Thr
59	Pro	Phe	Phe	Trp	Val	Leu
60	Pro	Phe	Phe	Trp	Val	Leu
61	Gly	Thr	Phe	Leu	Tyr	Thr
62	Gly	Thr	Phe	Leu	Tyr	Thr

cyclic peptide 1

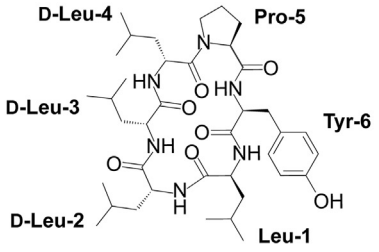

Fig. 2. Cyclic peptides studied in this work. The peptides are divided into three groups: Group 1 (Leu-rich), Group 2 (sequence variants) and Group 3 (orbitide-like), based on their amino acid composition. Each peptide's sequence is shown in three-letter code. N-methylated residues are indicated using gray shading. A chemical representation of peptide **1** is shown in the bottom left of the figure.

temperature coefficients ($\Delta\delta_{NH}/\Delta T$), which are non-destructive and convenient measures of the hydrogen bond network of a protein/peptide [36]. It has been proposed that backbone amides with very negative $\Delta\delta_{NH}/\Delta T$ (i.e. < -4.6 ppb/K) are solvent-exposed, whereas those with less negative or slightly positive $\Delta\delta_{NH}/\Delta T$ (i.e. ≥ -4.6 ppb/K) are considered to be involved in intra-molecular hydrogen bonds [37]. Panels A and B of Fig. 5 show the $\Delta\delta_{NH}/\Delta T$ for each amide of peptides 1 and 5, respectively, in 30% v/v acetonitrile. We measured $\Delta\delta_{NH}/\Delta T$ values for all 62 peptides and used these values to predict the number of intra-molecular hydrogen bonds for each peptide. However, there was no clear correlation between permeability and the combined number of intra-molecular hydrogen bonds and N-methyl groups, though a positive trend was emerging for permeability values measured using the Caco-2 assay (Supplementary Fig. 3). It is worth noting that the cut-off value of -4.6 ppb/K used in our analysis was proposed based on a study of proteins in water [37] and may not be appropriate for the small cyclic peptides in this study, which were dissolved in a buffer containing a percentage of organic solvent (though we investigate this issue in more detail later using molecular dynamics simulation). Nevertheless, we wondered whether the strength of each hydrogen bond might also be an important consideration.

Based on the above observations, we propose the $\Sigma\Delta\delta_{NH}/\Delta T$ value as a convenient overall measure of the hydrogen bonding potential of a peptide; examples of this value for peptides 1 and 5 are shown in Fig. 5A and B, respectively. In addition to calculating $\Sigma\Delta\delta_{NH}/\Delta T$ values for the peptides in 30% v/v acetonitrile, we further explored the utility of other solvent systems, i.e. 100% v/v

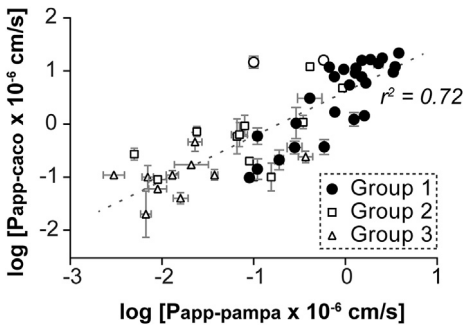

Fig. 3. Relationship between apparent permeability ($P_{app\text{-}caco}$) measured using the Caco-2 assay and apparent permeability ($P_{app\text{-}pampa}$) measured using PAMPA. The peptides used in this study are divided into three groups, defined in Fig. 2. The symbols of the three groups are shown in the inset; an empty circle belongs to Group 1 but represents peptides that have a recovery of less than 50% (see Supplementary Fig. 1). Logarithm values are shown as mean ± standard error of the mean. A linear correlation was fitted to permeability values (except for those with low recovery) is shown as a dotted line. The measured values are shown in Supplementary Table 1.

acetonitrile, 100% v/v chloroform, 10% v/v DMSO with 90% chloroform and 100% v/v DMSO, measuring $\Delta\delta_{NH}/\Delta T$ values for peptides from Group 1. We focused on Group 1 peptides because they were late-eluting but still showed varied permeability. Supplementary Fig. 4 shows the $\Sigma\Delta\delta_{NH}/\Delta T$ values plotted against Caco-2 and PAMPA permeability. Although a definitive correlation was not observed, a general relationship for some cases emerged, as shown in left panel of Supplementary Fig. 4C. Overall, these results encouraged us to investigate more sophisticated ways of utilizing $\Sigma\Delta\delta_{NH}/\Delta T$ values.

3.5. An experimental model of peptide permeability

We hypothesized that rather than assessing each parameter by itself, a combination of experimental parameters would provide more insight into the physico-chemical properties affecting peptide permeability. Indeed, analysis of the Caco-2 permeability of our peptides using the Quantitative Structure–Activity Relationship (QSAR) procedure showed that we could improve the agreement between observed and calculated log $P_{app\text{-}caco}$ by incorporating both log k′ and $\Sigma\Delta\delta_{NH}/\Delta T$ values in the calculation (Supplementary Table 4). For example, using log k′ alone in the calculations resulted in a r^2 of 0.62, and using $\Sigma\Delta\delta_{NH}/\Delta T$ values from samples in 30% v/v acetonitrile or 10% v/v DMSO, 90% v/v chloroform alone resulted in r^2 values of 0.22 or 0.15, respectively; whereas, using both input types resulted in an improvement in r^2 values, i.e. 0.64 and 0.70 for the combined use of log k′ and $\Sigma\Delta\delta_{NH}/\Delta T$ values for the two different solvent conditions mentioned above, respectively. An equation describing the permeability of Group 1 peptides can be formulated as follows:

$$\log P_{app-caco} = 0.54(\pm 0.08)\log k' + 0.21(\pm 0.08)\sum \Delta\delta_{NH}/\Delta T - 0.55(\pm 0.08)$$

$$n = 28,\ s = 0.41,\ r^2 = 0.70,\ q^2 = 0.63$$

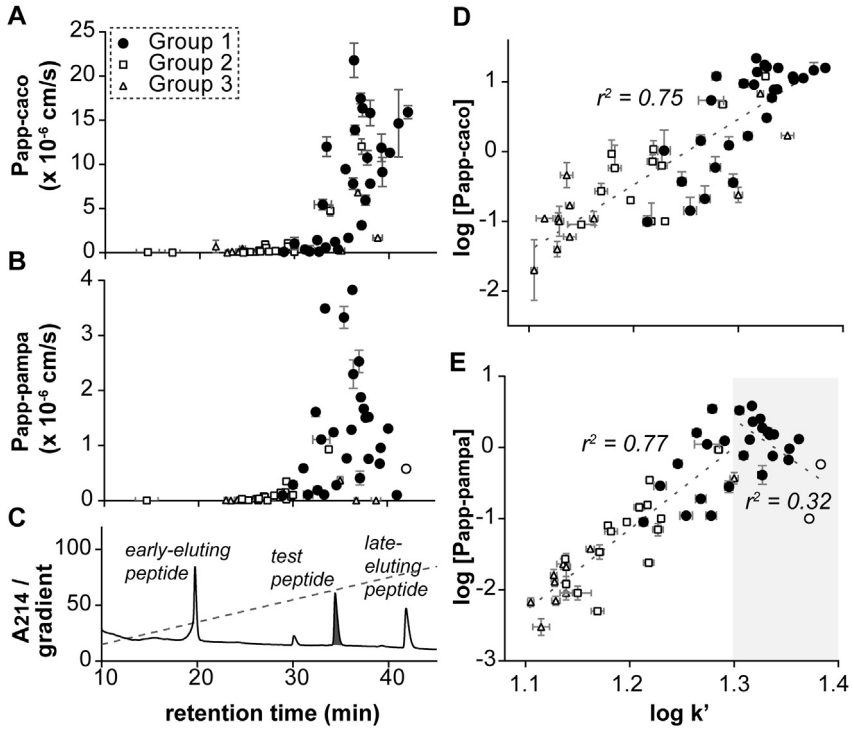

Fig. 4. Retention times of peptides as a marker of peptide permeability. Relationship between retention time measured using RP-HPLC and (A) apparent permeability ($P_{app\text{-}caco}$) measured using the Caco-2 assay or (B) apparent permeability ($P_{app\text{-}pampa}$) measured using PAMPA. The peptides are divided into three groups, defined in Fig. 2. The symbols of the three groups are shown in the inset in panel A; an empty circle belongs to Group 1 but represents peptides that have a recovery of less than 50% (see Supplementary Fig. 1). Values are shown as mean ± standard error of the mean. (C) A typical RP-HPLC chromatogram used to measure the retention time of peptides (see Supplementary information for traces of each peptide). Two internal standards were included in each run, an early-eluting and a late-eluting peptide (details in Methods). The peak of an example test peptide is shaded gray. A small peak eluting at ~30 min was observed, and is from an impurity from the DMSO used to dissolve the peptide samples, and not from the peptide synthesis and purification process (details in Supplementary results). The gradient (i.e. percentage of 90% v/v acetonitrile, 9.95% v/v water, 0.05% v/v TFA) used is shown as a dotted line. Relationship between the logarithm of the HPLC capacity factor (log k′) and (D) the logarithm of $P_{app\text{-}caco}$ or (E) $P_{app\text{-}pampa}$. A bilinear analysis was carried out for the PAMPA results; an r^2 of 0.77 was obtained for log k′ ≤ 1.3 and an r^2 of 0.32 for log k′ > 1.3. The shaded region in (E) represents the region with log k′ > 1.3. The capacity factors for the cyclic peptides are shown in Supplementary Table 2.

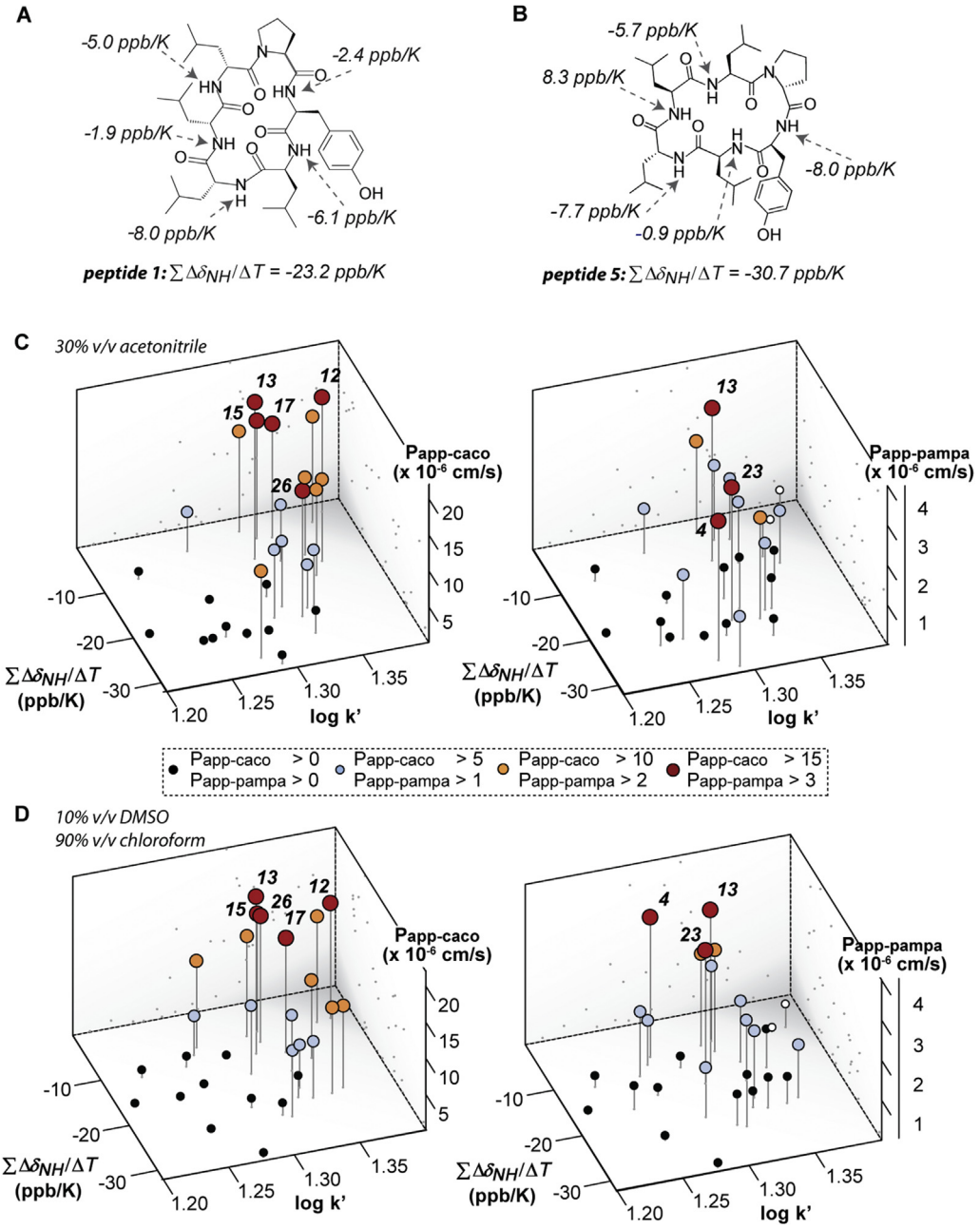

Fig. 5. Relationship between retention time, amide temperature coefficients, and permeability. A) Chemical structure of peptide **1** with the $\Delta\delta_{NH}/\Delta T$ values in 30% v/v acetonitrile for each amide indicated. B) Chemical structure of peptide **5** and the $\Delta\delta_{NH}/\Delta T$ values in 30% v/v acetonitrile. The summation of all $\Delta\delta_{NH}/\Delta T$ values ($\Sigma\Delta\delta_{NH}/\Delta T$) is shown for each peptide. Correlative plots for $\Sigma\Delta\delta_{NH}/\Delta T$ derived from 30% v/v acetonitrile, and 10% v/v DMSO with 90% v/v chloroform are shown in panels (B) and (D), respectively. In each panel, the leftmost plot corresponds to Caco-2 permeability measurements and the rightmost plot corresponds to PAMPA permeability measurements. Both apparent permeability (P_{app}) measured using the Caco-2 assay (left panels) and percent permeability (%P) measured using PAMPA (right panels) are divided into four levels depending on their mean permeability values, as indicated in the key at the bottom of the figure. Empty circles represent peptides that have a recovery of less than 50% (see Supplementary Fig. 1).

where *n* is the number of cyclic peptides, *s* is the standard error, *r* the correlation coefficient, *q* the cross-validated (leave-one-out) correlation coefficient, and the figures in parentheses are the standard error values for the coefficients or the constant. Similarly, QSAR analyses of the PAMPA permeability coefficients showed that using both log k′ and $\Sigma\Delta\delta_{NH}/\Delta T$ values provided more accurate predictions of log $P_{app\text{-}pampa}$ (Supplementary Table 4). For example, using log k′ or $\Sigma\Delta\delta_{NH}/\Delta T$ values (10% v/v DMSO, 90% v/v chloroform) alone in the calculations resulted in a r^2 of 0.05 and 0.24, respectively; however, using both molecular descriptors gave a r^2 of 0.57. Of the different solvent systems used to measure $\Sigma\Delta\delta_{NH}/\Delta T$ values, 100% v/v chloroform provide the best correlation in combination with log k′, with a r^2 of 0.68. This is interesting because chloroform is a weak hydrogen bond acceptor and is thus expected to have a relatively small effect on the proton resonance of solvent-exposed amides compared to strong hydrogen bond acceptors like DMSO. Perhaps the potential utility of chloroform as the solvent system for temperature coefficient measurements reflects its ability to mimic the interior of the lipid bilayer.

We also carried out a bilinear analysis to model the negative impact of high log k′ values on permeability, as exemplified in a study on the PAMPA permeability of hydrophobic compounds [34,35]. In general, the correlation was further improved using this type of analysis, resulting in equations similar to the following:

$$\log P_{app-pampa} = 3.10(\pm 1.42)\log k' + 0.24(\pm 0.06)\sum \Delta\delta_{NH}/\Delta T - 2.84(\pm 1.42)\log\left(\beta 10^{\log k'} + 1\right) - 0.08(\pm 0.06)$$

$$n = 26,\ s = 0.30,\ r^2 = 0.63,\ q^2 = 0.52$$

where the $\Sigma\Delta\delta_{NH}/\Delta T$ values, in this example, are measured using 10% v/v DMSO, 90% v/v chloroform, and $log\beta = -2.32$, as suggested in a previous study [34]. Here, cyclic peptides 12 and 16 were omitted from the analyses because their low recoveries (i.e. < 50%; Supplementary Fig. 1) would affect the accuracy of their observed permeability. Regardless of the type of QSAR model applied, the QSAR analyses performed herein demonstrate that both molecular descriptors, i.e. HPLC capacity factor and amide temperature coefficients, contribute to cyclic peptide permeability.

In addition to quantitative analyses, we carried out qualitative analyses of our permeability data. Fig. 5C and D and Supplementary Fig. 5 show the relationship between permeability (divided into four levels depending on the permeability value), retention time, and $\Sigma\Delta\delta_{NH}/\Delta T$ measured in four different solvent systems. Strikingly, the combination of retention time and $\Sigma\Delta\delta_{NH}/\Delta T$ value was generally able to resolve peptides with high permeability from peptides with low permeability, particularly for permeability measured using the Caco-2 assay, but this was not as noticeable for permeability measured by PAMPA. Specifically, peptides with very high permeability have high retention times and less negative $\Sigma\Delta\delta_{NH}/\Delta T$ values, whereas peptides with very low permeability have low retention times or very negative $\Sigma\Delta\delta_{NH}/\Delta T$ values, as shown in the left-hand panels of Fig. 5C and D.

3.6. Molecular simulations of peptide conformations in explicit solvent

To understand the molecular forces underpinning the observed relationship between retention time, $\Sigma\Delta\delta_{NH}/\Delta T$ values and permeability, we conducted molecular dynamics simulations of the peptides in explicit solvent (Fig. 6A) and monitored their molecular motion over 10 ns after an initial equilibration period. To validate our simulated structures we compared parameters measured *in silico* with parameters measured *in vitro* (Figs. 6 and 7). A positive correlation was observed between vLogP, an estimate of the n-octanol/water partition coefficient calculated from the peptide structures simulated in 30% v/v acetonitrile, and retention time ($r^2 = 0.70$; Fig. 6B), providing confidence in our computational method. We then measured surface properties of the peptides from their tertiary structures over the course of the simulation (Fig. 6C) and observed a stronger correlation between total hydrophobic surface area and retention time ($r^2 = 0.63$) than total polar surface area and retention time ($r^2 = 0.29$).

As $\Delta\delta_{NH}/\Delta T$ values have been used to predict hydrogen bonded amides within proteins, we investigated whether we could observe a relationship between $\Delta\delta_{NH}/\Delta T$ and the presence of a hydrogen bond within our peptides. Over the course of a molecular dynamics simulation for each peptide, we measured the frequency of each amide participating in an intra-molecular hydrogen-bond. Although amides frequently participating in an intra-molecular hydrogen-bond tended to have less negative $\Delta\delta_{NH}/\Delta T$ values (Supplementary Fig. 6A), a more prominent relationship was observed between $\Delta\delta_{NH}/\Delta T$ and the frequency of an amide participating in inter-molecular hydrogen bonds with solvent molecules (Fig. 7A and Supplementary Fig. 6B). Specifically, amides with very negative $\Delta\delta_{NH}/\Delta T$ values were frequently involved in hydrogen bond interactions with solvent, whereas

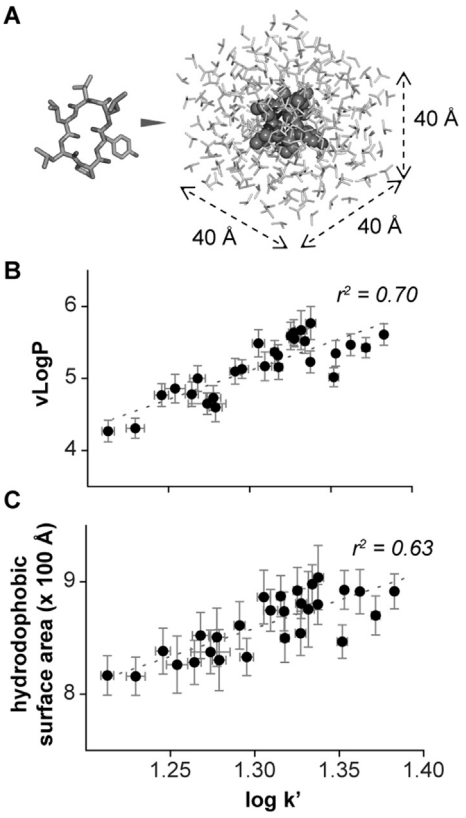

Fig. 6. Validation of molecular dynamics simulations of peptides. A) Peptides were subjected to molecular dynamics simulations in a defined box of explicit solvent. B) Correlation between observed retention time and calculated vLogP. C) Relationship between retention time and total hydrophobic surface area. Values of vLogP and total hydrophobic surface area are shown as mean ± standard deviation of all frames (10,000 frames) over the course of the production simulation.

amides with less negative $\Delta\delta_{NH}/\Delta T$ values were infrequently involved in solvent interactions. Interestingly, a strong correlation was observed between the $\Sigma\Delta\delta_{NH}/\Delta T$ values and the total frequency of all amides participating in solvent hydrogen-bonds for each peptide ($r^2 = 0.81$; Fig. 7B) and the total solvent-exposed surface area of the amide ($r^2 = 0.69$; Supplementary Fig. 6D). Overall, these results provide a structural basis for the measured $\Delta\delta_{NH}/\Delta T$ values.

We also carried out molecular dynamics simulations of the peptides in 100% v/v chloroform and 10% v/v DMSO with 90% v/v chloroform, and the results are summarized in Supplementary Fig. 7. In general, the overall conformation of the peptides remained similar across different solvents as shown in Supplementary Fig. 8, which is consistent with the idea that the cyclic backbone constrains the conformation of the peptides.

3.7. A computational model of peptide permeability

As a combination of experimental parameters was useful in resolving the physico-chemical properties of peptides that relate to permeability, we tested whether multiple computational parameters could also provide insight into the factors affecting peptide permeability. Supplementary Fig. 9 shows the relationship between vLogP, total solvent hydrogen bond frequency and permeability, as well as total hydrophobic surface area, total polar surface area and permeability. Peptides with high permeability tend to have high partition coefficients and few hydrogen bond interactions with water (Supplementary Fig. 9). Additionally, peptides with high

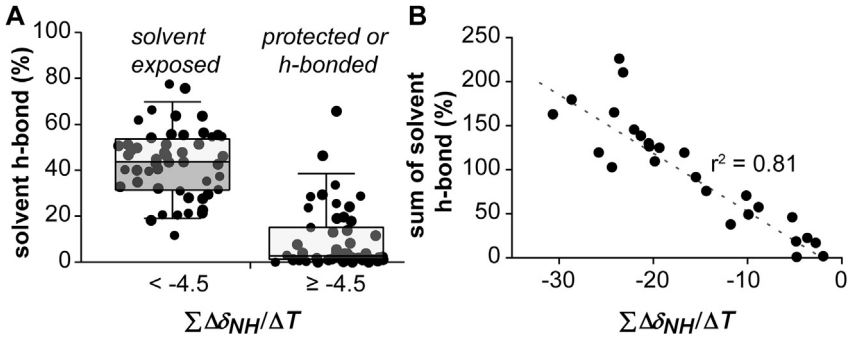

Fig. 7. Relationship between hydrogen bonding potential and NMR amide temperature coefficients. A) Relationship between $\Delta\delta_{NH}/\Delta T$ and the total frequency of inter-molecular solvent hydrogen bonds for all amides of each peptide. The amides are divided into two categories according to their $\Delta\delta_{NH}/\Delta T$ value. The box-plot (5–95 percentile) shows the distribution of the solvent hydrogen bonding frequency within each category. B) Relationship between $\Sigma\Delta\delta_{NH}/\Delta T$ and the total frequency of intra-molecular hydrogen bonds for all amides of each peptide.

permeability tend to have solvent exposed surfaces with larger hydrophobic and smaller polar content (Supplementary Fig. 9).

4. Discussion

There is an increasing focus in the pharmaceutical industry on the development of oral peptide therapeutics. In this study, we explored experimental and computational measures of peptide permeability to help guide medicinal chemists during peptide-based drug design. We assembled a library of 62 cyclic hexapeptides with varied *in vitro* permeability and, based on a systematic analysis of experimental markers, we developed a model that helps to explain the different permeability efficiencies of these peptides. Furthermore, we provided insight into the fundamental structural features described by the experimental biomarkers using molecular dynamics simulations in explicit solvent. We note that the results described herein relate primarily to passive transport of peptides across a cell barrier.

Initially we searched for a single experimental biomarker of peptide permeability. We found a striking relationship between the HPLC capacity factor and *in vitro* permeability (Fig. 4). We then found a correlation between the capacity factor and the predicted lipophilicity, suggesting that lipophilicity is an important determinant of peptide permeability. Lipophilicity is important likely because passive diffusion through the hydrophobic core of the lipid bilayer, which is a major constituent of the cell membrane, is promoted by increased peptide lipophilicity. This observation is consistent with previous observations [3,38], indicating that lipophilicity is a general property that affects permeability. Analysis of surface properties of simulated structures revealed that the retention times were also related to the surface hydrophobicity of the cyclic peptides (Fig. 6), which is consistent with studies on linear peptides and their retention times [39]. This correlation suggests that the total surface area of exposed hydrophobic atoms/residues is related to peptide lipophilicity and affects peptide permeability. Indeed, increasing the hydrophobicity of peptide **1** (retention time of 32.4 min) by replacing Tyr-6 with a Trp residue to produce peptide **23** (retention time of 35.4 min) resulted in a 7-fold increase in permeability across Caco-2 cells. Despite this finding, we observed that many peptides with high retention times still displayed poor permeability, suggesting that lipophilicity in isolation is not a sufficient descriptor of peptide permeability. In our experience, increasing lipophilicity alone as a strategy is detrimental to the delivery of orally efficacious drugs because it negatively impacts properties like solubility and metabolic stability; therefore, it is important to explore other properties that may impact bioavailability.

Looking beyond lipophilicity, we then considered the hydrogen bonding potential of the peptides following recent literature reports on the importance of intra-molecular and inter-molecular hydrogen bonds for cyclic peptides [10,15–17] and small molecules [40]. Specifically, structural studies of cell-permeable peptides have suggested that steric occlusion of polar groups and internal hydrogen bonding can lead to increased permeability [41,42]. Recognizing that hydrogen bonding potential is heavily dependent on conformation, we explored whether structural tools that can experimentally probe the hydrogen bond network can also be used as biomarkers of peptide permeability. We focused on amide temperature coefficients instead of hydrogen–deuterium exchange rates because amide temperature coefficients are easily measured in different solvent systems (i.e. composition and pH) and do not require temporal monitoring of the kinetics, though both techniques have been widely used to provide supplemental information on protein structure. Additionally, we were encouraged by our recent study, in which we showed that amide temperature coefficients could be used to guide the design and synthesis of N-methylated cyclic peptides that had small-molecule-like oral bioavailability [16]. Our previous study was based on the hypothesis that amide temperature coefficients could be used to identify appropriate amides for chemical modification. In this study, we showed, using molecular dynamics simulations, that amide temperature coefficients are a measure of the relative solvent exposure of amides (Fig. 7). Therefore, modification of exposed amides with N-methyl groups effectively caps these amides, reducing hydrogen bond interactions between the solvent and the peptide. However, in this study, we also found that peptides with similar hydrogen bonding potential could still display very different levels of permeability. For example, peptide **16** and **42** have the same N-methylation pattern (i.e. amides of residues 1, 2 and 4 were modified) and hydrogen bond network but the Caco-2 permeability of **16** is significantly higher than that of **42**. Therefore, hydrogen bonding potential alone is not a sufficient descriptor of peptide permeability.

We therefore considered the effect of both lipophilicity and hydrogen bonding potential on peptide permeability. Indeed, quantitative analyses of the permeability coefficients showed that both molecular descriptors contributed to permeability. On the basis of this result and our qualitative analyses, we propose our first model of peptide permeability based on experimentally measured parameters, as shown in Fig. 8A. Specifically, peptides with the highest permeability have high lipophilicity and few solvent interactions, whereas peptides with the lowest permeability have poor lipophilicity or many solvent interactions. The permeability of peptides with a moderate number of solvent interactions can be

improved by increasing its lipophilicity, which would partly compensate for the presence of unfavorable solvent interactions. The comparison of peptides **1** and **23** mentioned above is an example of this scenario. Similarly, the permeability of peptides with moderate lipophilicity can be improved by reducing the number of its hydrogen bond interactions with solvent. For example, the permeability of peptide **1** was improved by N-methylating its exposed amides to produce peptide **13**. It is worth noting that in some cases these two markers are related. For example, addition of N-methyl groups at appropriate locations not only reduces the number of solvent interactions but also increases lipophilicity (by increasing surface hydrophobicity).

Our first model can be applied to explain the derived correlations using Caco-2 permeability values (Fig. 5C and D, leftmost panels). The same trend is not as evident from correlations derived using PAMPA permeability values (Fig. 5C and D, rightmost panels), where peptides with the highest lipophilicities and fewest solvent interactions were not the most permeable. In fact, after a certain threshold, increasing lipophilicity appeared to be detrimental to permeability (Fig. 4E). We reason that an additional parameter is affecting our observed trends, namely solubility. With regard to peptides, increasing the lipophilicity would be expected to reduce solubility, as suggested recently [43] and as seen with small molecules [44], and thereby affect permeability. This is probably because increased lipophilicity might lead to peptide aggregation or sequester the peptides in the lipid membrane due to less favorable interactions in the aqueous phase. Indeed, this reduced solubility is reflected in the recovery rates, as shown in Supplementary Fig. 1. Increased lipophilicity leads to lower recovery rates; this effect is more pronounced for PAMPA measurements compared to Caco-2 measurements. Therefore, we propose our second model, shown in Fig. 8B, which defines an 'island of permeability' (shown in white). Peptides with lipophilicity and solvent interactions that lie on this 'island' are likely to have high permeability. This plot has similarities to the 'golden triangle' discussed by Johnson and colleagues [45], which focused on lipophilicity and molecular weight of small molecules.

We can rationalize our model using principles of thermodynamics. For peptides to permeate across a lipid bilayer, they must first insert into the bilayer; in other words, they must transition from one environment type, i.e. an aqueous environment with a high dielectric constant, to another, i.e. the bilayer core that would have a low dielectric constant. The principles underlying this transfer between two different environments is analogous to studies on partition of molecules between two different solvents [46]. For peptides, it has been proposed that the free energy of insertion (ΔG_I) of cyclic peptides into a lipid bilayer is strongly correlated to the logarithm of the PAMPA permeability coefficient. Additionally, it has been proposed that the transfer free energy is affected by the solvation free energy (ΔG_{solv}) [47], which describes changes in the solvation of the cyclic peptides upon partitioning and is composed of electrostatic contributions and non-polar contributions. Electrostatic contributions result from changes in the solvent dielectric constant and is affected by the peptide hydrogen bond network. As an example, the cost of transferring isolated *C=O* and *N–H* groups would be greater compared with a single hydrogen bond *C=O···N–H*. Non-polar contributions, or otherwise known as the classical hydrophobic effect, accounts for van der Waals and solvent structure effects. Although hydrophobicity can drive insertion of peptides into the lipid bilayer [47] it will also lead to decreased solubility in response to the cohesive energy of water [48]. As the lipid bilayer is a complex biomolecular system, it is likely that other energy-terms are also important, including lipid perturbation effects and contributions from peptide conformational changes.

The work described here provides a basis for future studies examining other features of peptides that might affect permeability, such as those proposed to affect small molecule permeability. Since Lipinski's seminal work [2], many features affecting small molecule permeability have been reported, including the ionization state [49,50], and molecular size and shape [3,45], which we have not considered in our study and thus there will be limitations to our model. We anticipate that our 'island' may shift for peptides with larger molecular weights than those used in this study. As reported for small molecules, an increased lipophilicity is required to obtain sufficient oral uptake as molecular weight increases [44]. A disadvantage of increasing lipophilicity of small molecules is that increased lipophilicity is known to be correlated to higher levels of target promiscuity [51], as well as increased risks of *in vivo* animal toxicity [52]. We speculate that structurally more complex macrocyclic peptides might enable increased selectivity, and therefore, the risks of increased lipophilicity could be lower than for oral small molecule drugs. Another encouraging observation is that the molecular weight of the cyclic peptide cyclosporine A, which is administered orally as an immunosuppressant, is above 1000 Da, signifying that oral bioavailability can be achieved for peptides with molecular weights beyond those studied here.

5. Conclusion

We have investigated the physico-chemical properties of cyclic peptides that relate to permeability. We focused on the effect of lipophilicity and solvent interactions and proposed an 'island of permeability' to help understand the features of peptides that contribute to their cell permeability and potential orally bioavailability. We employed experimental techniques that are fast and

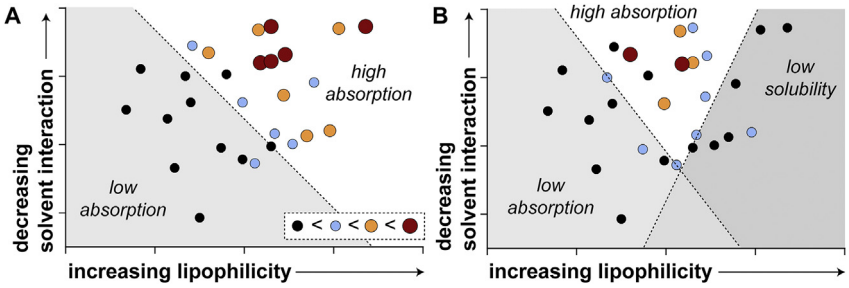

Fig. 8. An illustrative model for peptide permeability. A) Increasing lipophilicity and decreasing solvent interactions of peptides can lead to peptides with high absorption. Circles of different colors and sizes are used to represent different permeability levels (inset); peptides with the highest permeability are shown as red circles, whereas peptides with the lowest permeability are shown as black circles. This model can be applied to the correlations derived using our Caco-2 data (Fig. 5). B) In practice, increasing lipophilicity results in peptides with poor solubility, resulting in poor apparent permeability. The region in white defines an 'island of permeability', in which peptides are likely to have high permeability. (For interpretation of the references to color in this figure legend, the reader is referred to the web version of this article.)

convenient, recognizing the need for such methods in high-throughput drug design. We focused on molecular dynamics simulations to try and obtain accurate *in silico* models, though we expect that more rapid computational methods would also prove useful. Although it remains to be seen whether macrocyclic peptides will define a novel space of oral therapeutics, there are already encouraging signs from clinical drugs and candidates. A recent survey of macrocyclic drugs [53], of which macrocyclic peptides form a sub-class, revealed that 28% of registered macrocycles are delivered orally and 43% of clinical candidates are intended for oral administration. Although the examples of orally administered macrocyclic peptide drugs are still rare, we anticipate that more examples will be discovered and validated in the near future.

Funding sources

This work was supported by an ARC Linkage Grant (LP110200213) co-funded by Pfizer and a Queensland Government Smart Futures Co-investment Grant. CKW was supported by an National Health and Medical Research Council (NHMRC) Early Career Research Fellowship (546578). JES is an NHMRC Early Career Fellow (APP1069819). DJC is an NHMRC Professorial Fellow (APP1026501).

Acknowledgments

Caco-2 cells were kindly provided by Prof Istvan Toth. We thank Olivier Cheneval and Phillip Walsh for help with peptide synthesis.

Appendix A. Supplementary data

Supplementary data related to this article can be found at http://dx.doi.org/10.1016/j.ejmech.2015.04.049.

References

[1] D.J. Craik, D.P. Fairlie, S. Liras, D. Price, The future of peptide-based drugs, Chem. Biol. Drug Des. 81 (2013) 136–147.
[2] C.A. Lipinski, F. Lombardo, B.W. Dominy, P.J. Feeney, Experimental and computational approaches to estimate solubility and permeability in drug discovery and development settings, Adv. Drug Deliv. Rev. 46 (2001) 3–26.
[3] K. Valko, J. Butler, P. Eddershaw, Predictive approaches to increase absorption of compounds during lead optimisation, Expert Opin. Drug Discov. 8 (2013) 1225–1238.
[4] D.F. Veber, S.R. Johnson, H.Y. Cheng, B.R. Smith, K.W. Ward, K.D. Kopple, Molecular properties that influence the oral bioavailability of drug candidates, J. Med. Chem. 45 (2002) 2615–2623.
[5] J.E. Bock, J. Gavenonis, J.A. Kritzer, Getting in shape: controlling peptide bioactivity and bioavailability using conformational constraints, ACS Chem. Biol. 8 (2013) 488–499.
[6] C.T. Wong, D.K. Rowlands, C.H. Wong, T.W. Lo, G.K. Nguyen, H.Y. Li, J.P. Tam, Orally active peptidic bradykinin B1 receptor antagonists engineered from a cyclotide scaffold for inflammatory pain treatment, Angew. Chem. Int. Ed. Engl. 51 (2012) 5620–5624.
[7] R.J. Clark, J. Jensen, S.T. Nevin, B.P. Callaghan, D.J. Adams, D.J. Craik, The engineering of an orally active conotoxin for the treatment of neuropathic pain, Angew. Chem. Int. Ed. Engl. 49 (2010) 6545–6548.
[8] F.W. Okumu, G.M. Pauletti, D.G. Vander Velde, T.J. Siahaan, R.T. Borchardt, Effect of restricted conformational flexibility on the permeation of model hexapeptides across Caco-2 cell monolayers, Pharm. Res. 14 (1997) 169–175.
[9] J.G. Beck, J. Chatterjee, B. Laufer, M.U. Kiran, A.O. Frank, S. Neubauer, O. Ovadia, S. Greenberg, C. Gilon, A. Hoffman, H. Kessler, Intestinal permeability of cyclic peptides: common key backbone motifs identified, J. Am. Chem. Soc. 134 (2012) 12125–12133.
[10] T. Rezai, B. Yu, G.L. Millhauser, M.P. Jacobson, R.S. Lokey, Testing the conformational hypothesis of passive membrane permeability using synthetic cyclic peptide diastereomers, J. Am. Chem. Soc. 128 (2006) 2510–2511.
[11] J.F. Borel, C. Feurer, H.U. Gubler, H. Stahelin, Biological effects of cyclosporin A: a new antilymphocytic agent, Agents Actions 6 (1976) 468–475.
[12] J. Chatterjee, C. Gilon, A. Hoffman, H. Kessler, N-methylation of peptides: a new perspective in medicinal chemistry, Acc. Chem. Res. 41 (2008) 1331–1342.
[13] E. Biron, J. Chatterjee, O. Ovadia, D. Langenegger, J. Brueggen, D. Hoyer, H.A. Schmid, R. Jelinek, C. Gilon, A. Hoffman, H. Kessler, Improving oral bioavailability of peptides by multiple N-methylation: somatostatin analogues, Angew. Chem. Int. Ed. Engl. 47 (2008) 2595–2599.
[14] O. Ovadia, S. Greenberg, J. Chatterjee, B. Laufer, F. Opperer, H. Kessler, C. Gilon, A. Hoffman, The effect of multiple N-methylation on intestinal permeability of cyclic hexapeptides, Mol. Pharm. 8 (2011) 479–487.
[15] T.R. White, C.M. Renzelman, A.C. Rand, T. Rezai, C.M. McEwen, V.M. Gelev, R.A. Turner, R.G. Linington, S.S. Leung, A.S. Kalgutkar, J.N. Bauman, Y. Zhang, S. Liras, D.A. Price, A.M. Mathiowetz, M.P. Jacobson, R.S. Lokey, On-resin N-methylation of cyclic peptides for discovery of orally bioavailable scaffolds, Nat. Chem. Biol. 7 (2011) 810–817.
[16] C.K. Wang, S.E. Northfield, B. Colless, S. Chaousis, I. Hamernig, R.J. Lohman, D. Nielsen, C.I. Schroeder, S. Liras, D.A. Price, D.P. Fairlie, D.J. Craik, Rational design and synthesis of orally bioavailable peptides directed by NMR amide temperature coefficients, Proc. Natl. Acad. Sci. 111 (2014) 17504–17509.
[17] T. Rezai, J.E. Bock, M.V. Zhou, C. Kalyanaraman, R.S. Lokey, M.P. Jacobson, Conformational flexibility, internal hydrogen bonding, and passive membrane permeability: successful in silico prediction of the relative permeabilities of cyclic peptides, J. Am. Chem. Soc. 128 (2006) 14073–14080.
[18] X. Chen, A. Murawski, K. Patel, C.L. Crespi, P.V. Balimane, A novel design of artificial membrane for improving the PAMPA model, Pharm. Res. 25 (2008) 1511–1520.
[19] I.A. Lewis, S.C. Schommer, J.L. Markley, rNMR: open source software for identifying and quantifying metabolites in NMR spectra, Magn. Reson. Chem. 47 (Suppl. 1) (2009) S123–S126.
[20] W.F. Vranken, W. Boucher, T.J. Stevens, R.H. Fogh, A. Pajon, M. Llinas, E.L. Ulrich, J.L. Markley, J. Ionides, E.D. Laue, The CCPN data model for NMR spectroscopy: development of a software pipeline, Proteins 59 (2005) 687–696.
[21] C.K. Wang, S.E. Northfield, J.E. Swedberg, P.J. Harvey, A.M. Mathiowetz, D.A. Price, S. Liras, D.J. Craik, Translational diffusion of cyclic peptides measured using pulsed-field gradient NMR, J. Phys. Chem. B 118 (2014) 11129–11136.
[22] T. Herrmann, P. Guntert, K. Wuthrich, Protein NMR structure determination with automated NOE assignment using the new software CANDID and the torsion angle dynamics algorithm DYANA, J. Mol. Biol. 319 (2002) 209–227.
[23] E. Krieger, G. Koraimann, G. Vriend, Increasing the precision of comparative models with YASARA NOVA–a self-parameterizing force field, Proteins 47 (2002) 393–402.
[24] W. Humphrey, A. Dalke, K. Schulten, VMD: visual molecular dynamics, J. Mol. Graphics 14 (1996) 33–38, 27-38.
[25] K. Vanommeslaeghe, E. Hatcher, C. Acharya, S. Kundu, S. Zhong, J. Shim, E. Darian, O. Guvench, P. Lopes, I. Vorobyov, A.D. Mackerell Jr., CHARMM general force field: a force field for drug-like molecules compatible with the CHARMM all-atom additive biological force fields, J. Comput Chem. 31 (2010) 671–690.
[26] V. Zoete, M.A. Cuendet, A. Grosdidier, O. Michielin, SwissParam: a fast force field generation tool for small organic molecules, J. Comput. Chem. 32 (2011) 2359–2368.
[27] J.C. Phillips, R. Braun, W. Wang, J. Gumbart, E. Tajkhorshid, E. Villa, C. Chipot, R.D. Skeel, L. Kale, K. Schulten, Scalable molecular dynamics with NAMD, J. Comput. Chem. 26 (2005) 1781–1802.
[28] Z. Liu, G. Wang, Z. Li, R. Wang, Geometrical preferences of the hydrogen bonds on protein–ligand binding interface derived from statistical surveys and quantum mechanics calculations, J. Chem. Theory Comput. 4 (2008) 1959–1973.
[29] A. Pedretti, L. Villa, G. Vistoli, VEGA–an open platform to develop chemo-bio-informatics applications, using plug-in architecture and script programming, J. Comput. Aided Mol. Des. 18 (2004) 167–173.
[30] A.S. Konagurthu, J.C. Whisstock, P.J. Stuckey, A.M. Lesk, MUSTANG: a multiple structural alignment algorithm, Proteins 64 (2006) 559–574.
[31] P.G. Arnison, M.J. Bibb, G. Bierbaum, A.A. Bowers, T.S. Bugni, G. Bulaj, J.A. Camarero, D.J. Campopiano, G.L. Challis, J. Clardy, P.D. Cotter, D.J. Craik, M. Dawson, E. Dittmann, S. Donadio, P.C. Dorrestein, K.D. Entian, M.A. Fischbach, J.S. Garavelli, U. Goransson, C.W. Gruber, D.H. Haft, T.K. Hemscheidt, C. Hertweck, C. Hill, A.R. Horswill, M. Jaspars, W.L. Kelly, J.P. Klinman, O.P. Kuipers, A.J. Link, W. Liu, M.A. Marahiel, D.A. Mitchell, G.N. Moll, B.S. Moore, R. Muller, S.K. Nair, I.F. Nes, G.E. Norris, B.M. Olivera, H. Onaka, M.L. Patchett, J. Piel, M.J. Reaney, S. Rebuffat, R.P. Ross, H.G. Sahl, E.W. Schmidt, M.E. Selsted, K. Severinov, B. Shen, K. Sivonen, L. Smith, T. Stein, R.D. Sussmuth, J.R. Tagg, G.L. Tang, A.W. Truman, J.C. Vederas, C.T. Walsh, J.D. Walton, S.C. Wenzel, J.M. Willey, W.A. van der Donk, Ribosomally synthesized and post-translationally modified peptide natural products: overview and recommendations for a universal nomenclature, Nat. Prod. Rep. 30 (2013) 108–160.
[32] M. Bermejo, A. Avdeef, A. Ruiz, R. Nalda, J.A. Ruell, O. Tsinman, I. Gonzalez, C. Fernandez, G. Sanchez, T.M. Garrigues, V. Merino, PAMPA–a drug absorption in vitro model 7. Comparing rat in situ, Caco-2, and PAMPA permeability of fluoroquinolones, Eur. J. Pharm. Sci. 21 (2004) 429–441.
[33] S.K. Poole, C.F. Poole, Separation methods for estimating octanol-water partition coefficients, J. Chromatogr. B Anal. Technol. Biomed. Life Sci. 797 (2003) 3–19.
[34] M. Akamatsu, M. Fujikawa, K. Nakao, R. Shimizu, In silico prediction of human oral absorption based on QSAR analyses of PAMPA permeability, Chem. Biodivers. 6 (2009) 1845–1866.
[35] M. Fujikawa, K. Nakao, R. Shimizu, M. Akamatsu, QSAR study on permeability

of hydrophobic compounds with artificial membranes, Bioorg Med. Chem. 15 (2007) 3756–3767.
[36] V.J. Hruby, in: B. Weinstein (Ed.), Chemistry and Biochemistry of Amino Acids, Peptides and Proteins, Marcel Dekker, New York, 1974, 1–188.
[37] T. Cierpicki, J. Otlewski, Amide proton temperature coefficients as hydrogen bond indicators in proteins, J. Biomol. NMR 21 (2001) 249–261.
[38] A.C. Rand, S.S. Leung, H. Eng, C.J. Rotter, R. Sharma, A.S. Kalgutkar, Y. Zhang, M.V. Varma, K.A. Farley, B. Khunte, C. Limberakis, D.A. Price, S. Liras, A.M. Mathiowetz, M.P. Jacobson, R.S. Lokey, Optimizing PK properties of cyclic peptides: the effect of side chain substitutions on permeability and clearance, Medchemcomm 3 (2012) 1282–1289.
[39] B. Tripet, D. Cepeniene, J.M. Kovacs, C.T. Mant, O.V. Krokhin, R.S. Hodges, Requirements for prediction of peptide retention time in reversed-phase high-performance liquid chromatography: hydrophilicity/hydrophobicity of side-chains at the N- and C-termini of peptides are dramatically affected by the end-groups and location, J. Chromatogr. A 1141 (2007) 212–225.
[40] M. Fujikawa, R. Ano, K. Nakao, R. Shimizu, M. Akamatsu, Relationships between structure and high-throughput screening permeability of diverse drugs with artificial membranes: application to prediction of Caco-2 cell permeability, Bioorg. Med. Chem. 13 (2005) 4721–4732.
[41] W.M. Hewitt, S.S. Leung, C.R. Pye, A.R. Ponkey, M. Bednarek, M.P. Jacobson, R.S. Lokey, Cell-permeable cyclic peptides from synthetic libraries inspired by natural products, J. Am. Chem. Soc. 137 (2014) 715–721.
[42] D.S. Nielsen, H.N. Hoang, R.J. Lohman, T.A. Hill, A.J. Lucke, D.J. Craik, D.J. Edmonds, D.A. Griffith, C.J. Rotter, R.B. Ruggeri, D.A. Price, S. Liras, D.P. Fairlie, Improving on nature: making a cyclic heptapeptide orally bioavailable, Angew. Chem. Int. Ed. Engl. 53 (2014) 12059–12063.
[43] P. Thansandote, R.M. Harris, H.L. Dexter, G.L. Simpson, S. Pal, R.J. Upton, K. Valko, Improving the passive permeability of macrocyclic peptides: balancing permeability with other physicochemical properties, Bioorg. Med. Chem. 23 (2015) 322–327.
[44] M.J. Waring, Defining optimum lipophilicity and molecular weight ranges for drug candidates-Molecular weight dependent lower logD limits based on permeability, Bioorg. Med. Chem. Lett. 19 (2009) 2844–2851.
[45] T.W. Johnson, K.R. Dress, M. Edwards, Using the Golden Triangle to optimize clearance and oral absorption, Bioorg. Med. Chem. Lett. 19 (2009) 5560–5564.
[46] K. Goss, Free energy of transfer of a solute and its relation to the partition constant, J. Phys. Chem. B 107 (2003) 14025–14029.
[47] N. Ben-Tal, A. Ben-Shaul, A. Nicholls, B. Honig, Free-energy determinants of alpha-helix insertion into lipid bilayers, Biophys. J. 70 (1996) 1803–1812.
[48] R.L. Baldwin, The new view of hydrophobic free energy, FEBS Lett. 587 (2013) 1062–1066.
[49] M.P. Gleeson, Generation of a set of simple, interpretable ADMET rules of thumb, J. Med. Chem. 51 (2008) 817–834.
[50] D.T. Manallack, R.J. Prankerd, G.C. Nassta, O. Ursu, T.I. Oprea, D.K. Chalmers, A chemogenomic analysis of ionization constants–implications for drug discovery, ChemMedChem 8 (2013) 242–255.
[51] P.D. Leeson, B. Springthorpe, The influence of drug-like concepts on decision-making in medicinal chemistry, Nat. Rev. Drug Discov. 6 (2007) 881–890.
[52] J.D. Hughes, J. Blagg, D.A. Price, S. Bailey, G.A. Decrescenzo, R.V. Devraj, E. Ellsworth, Y.M. Fobian, M.E. Gibbs, R.W. Gilles, N. Greene, E. Huang, T. Krieger-Burke, J. Loesel, T. Wager, L. Whiteley, Y. Zhang, Physiochemical drug properties associated with in vivo toxicological outcomes, Bioorg Med. Chem. Lett. 18 (2008) 4872–4875.
[53] F. Giordanetto, J. Kihlberg, Macrocyclic drugs and clinical candidates: what can medicinal chemists learn from their properties? J. Med. Chem. 57 (2014) 278–295.